Cubane-Type [Mo_3S_4M] Clusters with First-Row Group 4-10 Transition-Metal Halides Supported by C_5Me_5 Ligands on Molybdenum

Yasuhiro Ohki,*[a] Keisuke Uchida,[a] Ryota Hara,[a] Mami Kachi,[a] Mayu Fujisawa,[a] Mizuki Tada,[a,b] Yoichi Sakai,[c] and W. M. C. Sameera[d]

Dedication ((optional))

Abstract: A synthetic protocol was developed for a series of cubane-type [Mo_3S_4M] clusters that incorporate halides of first-row transition metals from group 4-10 (M). This protocol is based on the anionic cluster platform [$Cp^*_3Mo_3S_4$]$^-$ ([**1**]$^-$; Cp^* = η^5-C_5Me_5), which crystallizes when K(18-crown-6) is used as the counter-cation. Treatment of *in-situ*-generated [**1**]$^-$ with such transition-metal halides led to the formation of [Mo_3S_4M] clusters, in which the M:halide ratio gradually changes from 1:2 to 1:1.5 and to 1:1, when moving from early to late transition metals. This trend suggests a tendency for early transition metals to tolerate higher oxidation states and adopt larger ionic radii relative to late transition metals. The properties of the [Mo_3S_4Fe] cluster **6a** were investigated in detail using ^{57}Fe Mössbauer spectroscopy and computational methods.

Introduction

Cubic [M_4S_4] clusters are a representative class of metal-sulfur compounds, whose major role is to mediate redox processes without significantly changing their structures.[1,2] Moreover, catalytic activity has been reported.[3] For instance, some biological [Fe_4S_4] clusters that carry a non-cysteinyl ligand form the catalytic centers of aconitase and IspG for biological reactions.[4,5] The cysteine-supported [Fe_4S_4] clusters in the Fe-proteins of *Azotobacter vinerandii* and *Methanosarcina acetivorans* catalyze the reductions of CO_2 to CO[6a] as well as of CO_2 to CO and hydrocarbons,[6b] respectively, and the turnover number (TON) of the latter reaction was increased with the synthetic [Fe_4S_4] cluster, [$Fe_4S_4(SCH_2CH_2OH)_4$]$^{2-}$.[6b] Some synthetic [M_4S_4] clusters have also been applied successfully as catalyst precursors. For instance, Coucouvanis *et al.* have reported that the Mo centers of cubane-type [Fe_3S_4Mo] clusters catalyze the reductions of N_2H_4, dimethyldiazene, and alkynes.[7] The groups of Tanaka, Tezuka, and Hidai have reported electro-catalytic reductions of CO_2, nitriles, isonitriles, and azides, in the presence of the cubane-type [Fe_3S_4Mo] or [Fe_4S_4] clusters.[8] Hidai *et al.* have discovered that the Pd and Ni centers of [Mo_3S_4M'] clusters (M' = Pd, Ni) catalyze the intramolecular cyclization of alkynoic acids and aminoalkynes,[9] and that an analogous [Mo_3S_4Ru] cluster catalyzes the disproportionation of N_2H_4.[10] Qu *et al.* have applied a [Mo_3S_4Pd]-(η^3-allyl) cluster to the catalytic conversion of allylic alcohols.[11] Llusar, Pérez-Prieto, and their co-workers have synthesized diphosphine-supported [Mo_3S_4Cu] clusters as catalysts for the intra- and inter-molecular cyclopropanation of alkenes,[12] while Llusar *et al.* have demonstrated the catalytic conversion of nitroarenes with a diamine-supported [Mo_3S_4Pt] cluster.[13] Therefore, the synthesis of various cubane-type clusters with a potential reaction site should expand the utility of such metal-sulfur compounds in bio-inspired and homogeneous catalysis.[14]

A platform class that has already been employed in the synthesis of previously reported [Mo_3S_4M'] (M' = groups 8-10 metals and group 6 carbonyls) clusters are the cationic Mo_3 clusters of the type [(η^5-C_5H_4Me)$_3Mo_3S_4$]$^+$ and [$Cp^*_3Mo_3S_4$]$^+$ ([**1**]$^+$; Cp^* = η^5-C_5Me_5).[15] However, in our preliminary investigations, the latter did not engage in any reactions with early transition metal halides such as $TiCl_3(THF)_3$, $NbCl_3(DME)$, or $MoCl_3(THF)_3$, demonstrating the limitations with respect to the range of metal halides that can be incorporated. On the other hand, we have recently discovered that the anionic cluster [$Cp^*_3Mo_3S_4$]$^-$ [**1**]$^-$ reacts with $TiCl_3(THF)_3$ to furnish $Cp^*_3Mo_3S_4TiCl_2$ (**2**), wherein the Ti atom activates N_2 upon treatment with KC_8.[16] Herein, we demonstrate that our synthetic protocol based on the cluster anion [$Cp^*_3Mo_3S_4$]$^-$ [**1**]$^-$ is versatile and able to accommodate first-row transition-metal halides of group 4-10 to provide a series of cubane-type clusters through salt-metathesis reactions.

[a] Prof. Y. Ohki, K. Uchida, R. Hara, M. Kachi, M. Fujisawa, Prof. M. Tada
Department of Chemistry, Graduate School of Science and Research Center for Materials Science, Nagoya University, Furo-cho, Chikusa-ku, Nagoya 464-8602 (Japan)
E-mail: ohki@chem.nagoya-u.ac.jp
[b] Prof. M. Tada
Research Center for Materials Science (RCMS) & Integrated Research Consortium on Chemical Sciences (IRCCS), Nagoya University, Furo-cho, Chikusa-ku, Nagoya 464-8602 (Japan)
[c] Prof. Y. Sakai
Department of Chemistry, Daido University, Takiharu-cho, Minami-ku, Nagoya 457-8530, Japan
[d] Prof. W. M. C. Sameera
Institute of Low Temperature Science, Hokkaido University, Sapporo 060-0819, Japan

Supporting information for this article is given via a link at the end of the document.

Results and Discussion

Crystallization and Characterization of the Anionic Mo_3 Cluster Platform.

In our recent study,[16] the cubane-type $[Mo_3S_4Ti]$ cluster $Cp^*_3Mo_3S_4TiCl_2$ (**2**) was synthesized from the cluster anion $[Cp^*_3Mo_3S_4]^-$ $[\mathbf{1}]^-$, which was generated *in-situ* by treatment of the neutral cluster $Cp^*_3Mo_3S_4$ (**1**) with 1 equiv of sodium naphthalenide in THF. In this study, the cluster anion was successfully isolated in 56% yield as dark green crystals of [K(18-crown-6)][**1**]$^-$, from the reaction of **1** with equimolar amounts of 18-crown-6 and KC_8 (Scheme 1). Single crystals of [Na(crown-ethers)][**1**] suitable for X-ray crystallographic analysis were not obtained from the analogous reactions of $Cp^*_3Mo_3S_4$ with sodium naphthalenide in the presence of 18-crown-6, 15-crown-5, or 12-crown-4, possibly due to the high solubility of $[\mathbf{1}]^-$ with a sodium counter-cation. Due to its paramagnetic properties, the ^{1}H NMR spectrum of $[\mathbf{1}]^-$ in THF-$[D_8]$ exhibited a broad Cp* signal at 13.3 ppm ($w_{1/2}$ = 44 Hz). The solution magnetic moment based on the Evans method was estimated as μ_{eff} = 2.3 μ_B at 297 K, which is indicative of the triplet S = 1 state.

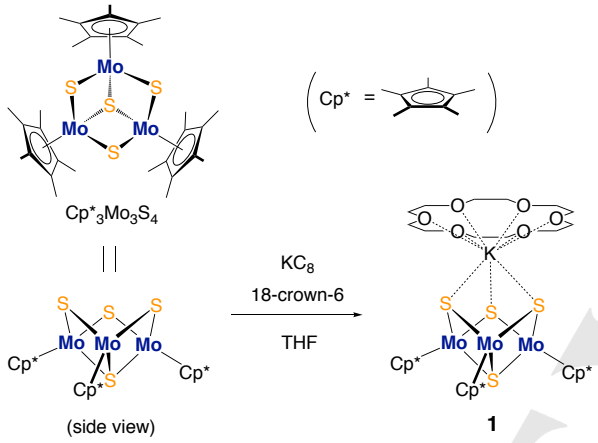

Scheme 1. Synthesis of [K(18-crown-6)][$Cp^*_3Mo_3S_4$] (**1**).

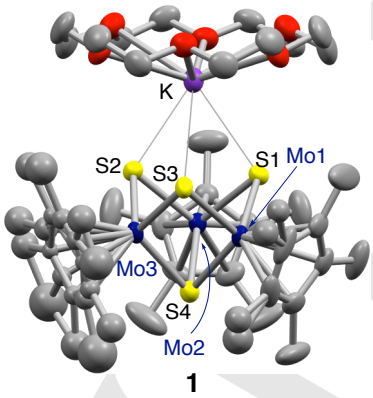

Figure 1 Molecular structure of **1** with atomic displacement parameters set at 50% probability. Only selected atoms are labeled, and hydrogen atoms are omitted for clarity. Isotopic refinement was applied to the carbon atoms of the disordered Cp* ligand. Selected distances (Å): Mo1-Mo2, 2.8530(4); Mo1-Mo3, 2.8555(4); Mo2-Mo3, 2.8574(4); Mo1-S1, 2.3456(11), Mo1-S3, 2.3392(9); Mo1-S4, 2.3419(9); Mo2-S1, 2.3420(10); Mo2-S2, 2.3443(10), Mo2-S4, 2.3448(8); Mo3-S2, 2.3462(11); Mo3-S3, 2.3393(9); Mo3-S4, 2.3436(9); K-S1, 3.2745(13); K-S2, 3.2612(13); K-S3, 3.4115(11).

The structure of [K(18-crown-6)][**1**]$^-$ was determined by a single-crystal X-ray diffraction analysis that revealed interactions between the anionic $[Cp^*_3Mo_3S_4]^-$ core and the cationic [K(18-crown-6)] moiety, which results in the formation of a pseudo-cubane structure (Figure 1). This structure allows a structural comparison with the cationic/neutral forms ($[Cp^*_3Mo_3S_4]^{+/0}$) that have previously been reported. The Mo-(μ_2-S) bond lengths consistently increase with sequential reductions, *i.e.*, the mean Mo-(μ_2-S) distance of neutral $Cp^*_3Mo_3S_4$ (2.309(6) Å)[17] is in between those of the cation $[Cp^*_3Mo_3S_4]^+$ (2.297(1) Å)[15] and the anion [K(18-crown-6)][$Cp^*_3Mo_3S_4$] (2.343(1) Å). On the other hand, the mean Mo-Mo bond length increases from 2.819(5) to 2.861(6) Å upon 1e reduction of the cation $[Cp^*_3Mo_3S_4]^+$, while a further 1e$^-$ reduction to the anionic form $[\mathbf{1}]^-$ leads to a comparable Mo-Mo distance (2.8553(4) Å).

According to an extended Hückel MO calculation on the simplified neutral cluster $(C_5H_5)_3Mo_3S_4$, an unpaired electron is stored in one of the doubly degenerate Mo d-type orbitals, which are anti-bonding with respect to both the Mo-Mo and Mo-S bonds.[17] This analysis is in agreement with the elongation of the Mo-Mo and Mo-S distances upon 1e$^-$ reduction of the cation $[Cp^*_3Mo_3S_4]^+$ to the neutral $Cp^*_3Mo_3S_4$, but inconsistent with the comparable Mo-Mo distances of anion $[\mathbf{1}]^-$ relative to the neutral form. In order to evaluate the electronic properties of the anionic cluster $[Cp^*_3Mo_3S_4]^-$, theoretical analyses were carried out for both cation-free $[Cp^*_3Mo_3S_4]^-$ and [K(18-crown-6)][$Cp^*_3Mo_3S_4$].

Three spin states (S = 0, 1, and 2) were fully optimized for cation-free $[Cp^*_3Mo_3S_4]^-$ (Table S2). According to the results at the B3LYP-D3BJ (20 Hatree Fock (HF)% exchange) level of theory, the triplet state (S = 1) is the ground state of $[Cp^*_3Mo_3S_4]^-$, while the singlet (S = 0) and quintet (S = 2) states are 7.9 kcal/mol and 20.2 kcal/mol above the ground state. In the ground state (S = 1), the calculated $\langle S^2 \rangle$ value (2.03) is consistent with the ideal value (2.00), implying no spin contamination. The amount of the HF exchange of the chosen density functional is known to be sensitive to the energy differences of the spin states and the spin-density distributions of transition metal complexes and clusters.[18] Therefore, we also used BP86-D3BJ (0 HF% exchange) to calculate the S = 0, 1, and 2 states of $[Cp^*_3Mo_3S_4]^-$. The results at the BP86-D3BJ level of theory suggest that the S = 1 state is the ground state, while the S = 0 state is only 0.3 kcal/mol higher in energy in this case. Nevertheless, the results at the B3LYP-D3BJ (20 HF%) and BP86-D3BJ (0 HF%) level of theory suggest that the S = 1 state is the ground state for $[Cp^*_3Mo_3S_4]^-$.

A similar electronic structure was found for [K(18-crown-6)][$Cp^*_3Mo_3S_4$], where the S = 1 state is the ground state (Table S3). This result is consistent with the solution magnetic moment of [K(18-crown-6)][**1**]$^-$ at 297 K. Based on the B3LYP-D3BJ functional, the S = 0 and 2 states of [K(18-crown-6)][**1**]$^-$ are 8.7 and 19.7 kcal/mol above the ground state, respectively. These

numbers are analogous to those for cation-free [**1**]$^-$, indicating a limited influence of interactions between the cluster anion and the [K(18-crown-6)] cation on the spin states. In the optimized *S* = 1 ground state of [K(18-crown-6)][**1**]$^-$, the calculated average Mo-Mo distance (2.92 Å) is slightly longer than that in the X-ray structure (2.8553(4) Å). The calculated mean Mo-(μ_2-S) distance (2.36 Å) is in good agreement with that obtained from the crystallographic analysis (2.343(1) Å). In the case of the cation-free [**1**]$^-$ system in the *S* = 1 state, the calculated average Mo-Mo and Mo-S distances are 2.92 Å and 2.34 Å, respectively, which are comparable to those calculated for the optimized *S* = 1 ground state of [K(18-crown-6)][**1**]$^-$. This result suggests a minor impact of the [K(18-crown-6)]$^+$ cation on the Mo-Mo and Mo-S distances. The reason for the comparable Mo-Mo distances in the crystal structure of [K(18-crown-6)][**1**]$^-$ and that of neutral **1** remains thus unclear, while the structural differences between the crystallographic and DFT-optimized structures might be attributed to the packing effects. It should also be noted that *ca.* 0.05 Å difference can be expected as errors in theory.

A ΔE value of 42 kcal/mol was calculated for the dissociation of [K(18-crown-6)]$^+$ from [K(18-crown-6)][**1**]$^-$ in THF, and therefore charge separation in solution should be unfavorable. The retention of the interaction betwen [K(18-crown-6)]$^+$ and [Cp*$_3$Mo$_3$S$_4$]$^-$ in solution was further supported by cyclic voltammetry menasurement of [K(18-crown-6)][**1**]$^-$ in THF. As shown in Figure 2, [K(18-crown-6)][**1**]$^-$ (red trace) exhibited the reversible redox processes across the triad states [Cp*$_3$Mo$_3$S$_4$]$^{+/0/-}$ at $E_{1/2}$ = –0.21 V ([Cp*$_3$Mo$_3$S$_4$]$^{+/0}$) and –1.00 V ([Cp*$_3$Mo$_3$S$_4$]$^{0/-}$), as well as an additional reversible process at $E_{1/2}$ = –2.50 V ([Cp*$_3$Mo$_3$S$_4$]$^{-/2-}$). The voltammogram also exhibited weak and reversible features at $E_{1/2}$ = –1.26 V and –2.26 V, which correspond to the [Cp*$_3$Mo$_3$S$_4$]$^{+/0}$ and [Cp*$_3$Mo$_3$S$_4$]$^{0/-}$ processes observed in the voltammogram of neutral **1** (blue trace). These results indicate that only a part of the [K(18-crown-6)] moieties dissociates from the Mo$_3$ cluster in solution, and that the interaction between [K(18-crown-6)] and the cluster anion [Cp*$_3$Mo$_3$S$_4$]$^-$ leads to a positive potential shift by >1.0 V for the [Cp*$_3$Mo$_3$S$_4$]$^{+/0}$ and [Cp*$_3$Mo$_3$S$_4$]$^{0/-}$ processes.

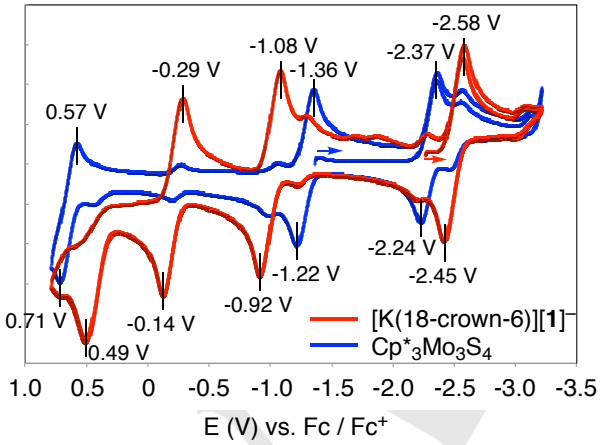

Figure 2 Cyclic voltammogram of [K(18-crown-6)][**1**]$^-$ (red) and Cp*$_3$Mo$_3$S$_4$ (**1**, blue) in THF; supporting electrolyte: 0.2 M [^{n}Bu$_4$N][PF$_6$]; scan rate: 100 mV/s. Weak features in the red and blue traces indicate the generation of potassium-free Cp*$_3$Mo$_3$S$_4$ (red) or contamination of the potassium-bound [Cp*$_3$Mo$_3$S$_4$]$^-$ (blue), while the relatively strong feature at *ca.* –2.5 V (blue) may result from the reduction of [^{n}Bu$_4$N][Cp*$_3$Mo$_3$S$_4$], which possibly has a strong interaction between [^{n}Bu$_4$N]$^+$ and [Cp*$_3$Mo$_3$S$_4$]$^-$.

Synthesis of Cubane-Type [Mo$_3$S$_4$M] Clusters.

A series of cubane-type clusters, *i.e.*, Cp*$_3$Mo$_3$S$_4$TiCl$_2$ (**2**), {Cp*$_3$Mo$_3$S$_4$M}$_2$(μ-Cl)$_3$ (M = V (**3**); M = Cr (**4**)), and Cp*$_3$Mo$_3$S$_4$MX (M = Mn, X = Cl (**5**); M = Fe, X = Cl (**6a**); M = Fe, X = Br (**6b**); M = Co, X = Cl (**7**); M = Ni, X = Br (**8**)), were synthesized by sequential reactions of Cp*$_3$Mo$_3$S$_4$ with Na(C$_{10}$H$_8$) and transition-metal halides (Scheme 2). The ratio between the hetero-metal (M) and the halide(s) (X) gradually increases from early to late transition metals, *i.e.*, M:X = 1:2 (Ti), 1:1.5 (V and Cr), and 1:1 (Mn, Fe, Co, and Ni). Thus, the products containing V and Cr appear as the chloride-bridged dimers with an integer M:X ratio (2:3), while the other products were obtained as monomers. The isolated yields were moderate (50-70%) for M = Ti, V, Fe, Co, and Ni, while that for M = Mn was low (11%) and only trace amounts were obtained for M = Cr. Varying the alkaline metal that accompanies the [Cp*$_3$Mo$_3$S$_4$]$^-$ anion does not seem to affect the yields of the resulting cubane-type clusters, *e.g.* the yield of [Mo$_3$S$_4$Co] cluster **7** from a mixture of Cp*$_3$Mo$_3$S$_4$ and Na(C$_{10}$H$_8$) (66%) is similar to that from [K(18-crown-6)][Cp*$_3$Mo$_3$S$_4$] (69%). Varying the halides did not affect the yields either, at least in the case of the [Mo$_3$S$_4$Fe] clusters **6a** (Cl, 66%) and **6b** (Br, 67%). The use of FeCl$_3$ instead of FeCl$_2$ resulted in the formation of a green/dark brown complex mixture, from which we were unable to isolate **6a**. Based on the color of the mixture, we speculate that a part of [**1**]$^-$ reduced FeCl$_3$ to furnish [**1**]$^{0/+}$ and FeCl$_2$. Even though a subsequent reaction of the remaining [**1**]$^-$ and *in-situ*-generated FeCl$_2$ may have generated small amounts of **6a**, we were unable to isolate any. The presence of Mo$_3$ clusters in the reaction mixture was indicated by the green color, which is common for clusters of the type [**1**]$^{-/0/+}$. The low yield of the [Mo$_3$S$_4$Mn] cluster **5** is probably due to the low solubility of MnCl$_2$ in THF, which should leads to an inappropriate ratio of the reactants in solution. In fact, a powder of unreacted MnCl$_2$ remained after stirring the reaction mixture overnight at room temperature. In the synthesis of the [Mo$_3$S$_4$Ni] cluster **8**, the commercially available bromide complex NiBr$_2$(DME) was chosen as the precursor by considering its solubility in THF, while analogous reactions with NiCl$_2$ or NiCl$_2$(DME) were not examined. Even though the 2:3:2 ratio of Cp*$_3$Mo$_3$S$_4$, Na(C$_{10}$H$_8$), and VCl$_3$(THF)$_3$ seems suitable for the synthesis of the [Mo$_3$S$_4$V] dimer **3**, this ratio furnished a lower yield (24%) relative to that obtained from the reaction under 1:1:1 ratio of the reactants (51%). Even though various amounts of Na(C$_{10}$H$_8$) were tested for the synthesis of [Mo$_3$S$_4$Cr] dimer **4**, the yield could not be improved. The synthesis of **4** via an analogous reaction using CrCl$_3$ instead of CrCl$_2$ has so far been unsuccessful, and the specific reason(s) for the low product yield remain unclear so far, even though the reaction has been subjected to several modifications (e.g. changing the ratio of the

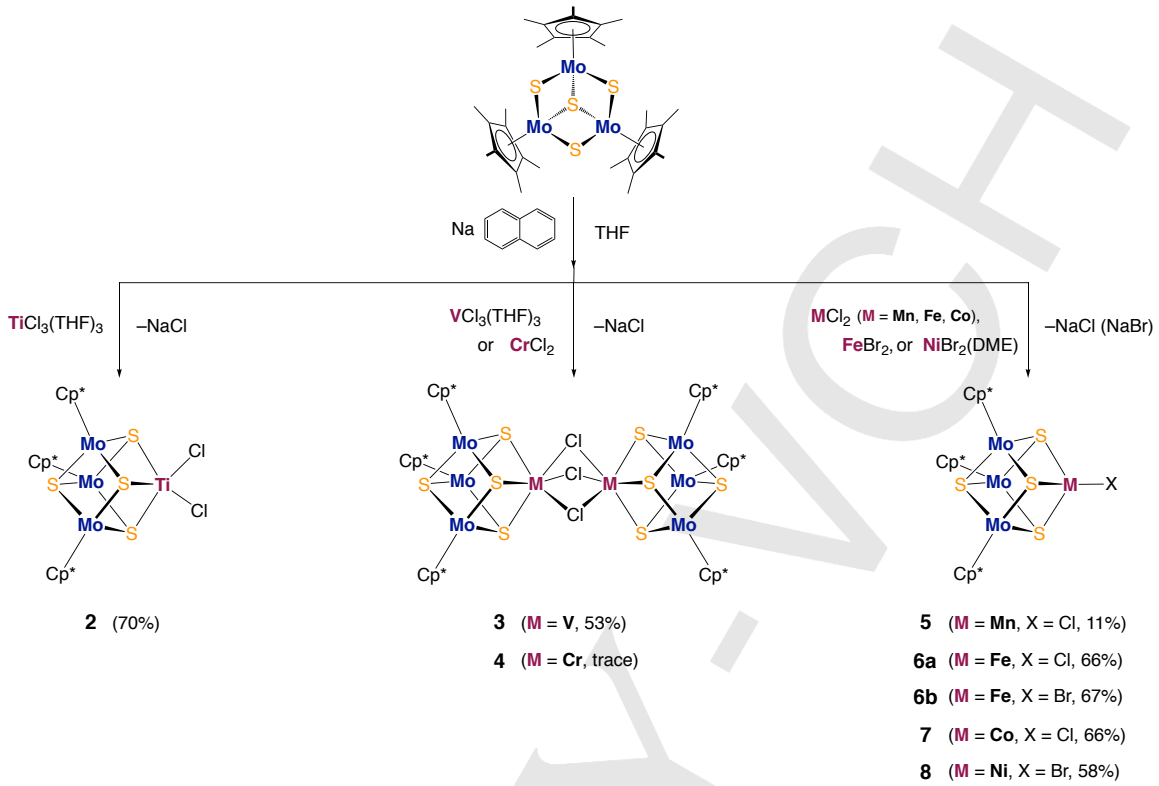

Scheme 2. Synthesis of Cubane-Type $[Mo_3S_4M]$ Clusters (M = Ti, V, Cr, Mn, Fe, Co, Ni).

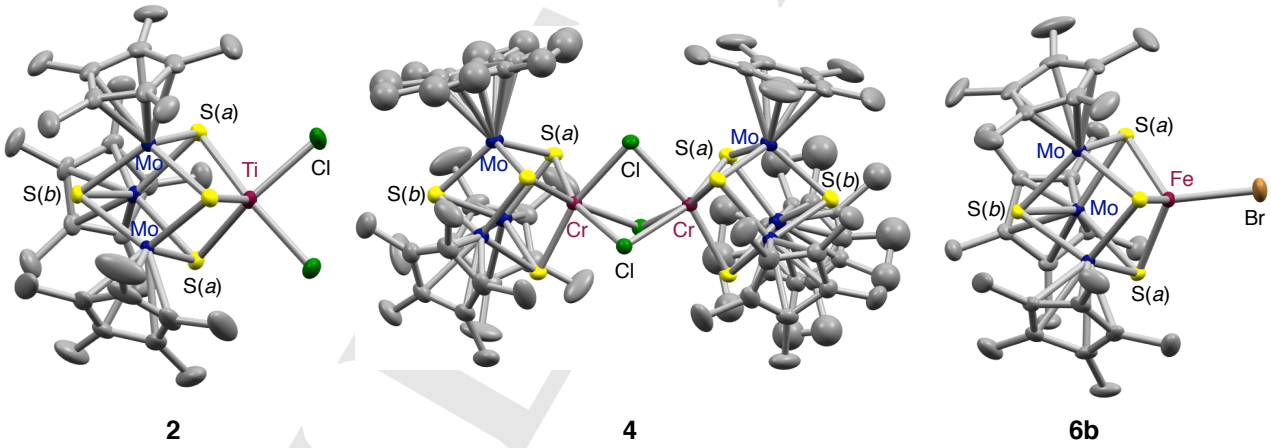

Figure 3 Molecular structures of **2**, **4**, and **6b** with atomic displacement parameters set at 50% probability. Only selected atoms are labeled, and hydrogen atoms are omitted for clarity. An isotopic refinement was applied to the carbon atoms of the disordered Cp* ligands.

reactants). Accordingly, **4** has been characterized only by X-ray crystallographic analysis.

Structures of Cubane-Type Clusters.

The molecular structures of all cubane-type clusters **2**-**8** were determined by single-crystal X-ray crystallography. Representative structures of **2**, **4**, and **6b** are shown in Figure 3, while other structures appear in the supporting information (Figures S1-S5). Selected bond distances in **2**-**8** are listed in Table 1. Although the $[Cp^*_3Mo_3S_4]^-$ platform was used as a tridentate ligand for hetero-metal M, this platform is not a simple metallo-ligand but constitutes the cubic $[Mo_3S_4M]$ core with M, as the observed Mo-M distances are indicative of Mo-M interactions particularly when M is a late transition metal.

The trend of the M:X ratio in **2**-**8** indicates larger ionic radiii and higher valency for early transition metals compared to late transition metals. The gradual decrease in the radius of M is compensated by a shortening of the Mo-M and M-$S_{(a)}$ distances upon ascending the position in the periodic system of the elements, although the fluctuations found in these distances

Table 1 Selected Bond Distances (Å) of the Cubic Clusters **2**-**8**.

	2	**3**	**4**	**5**	**6a**	**6b**	**7**	**8**
M	Ti	V	Cr	Mn	Fe	Fe	Co	Ni
Mo-M	3.0678(6)	2.7929(9)	2.8753(6)	2.9182(7)	2.7777(6)	2.7951(5)	2.7775(6)	2.7219(7)
	2.9951(5)	2.7987(9)	2.9089(6)	2.9182(7)	2.7777(6)	2.7949(5)	2.7783(6)	2.7366(6)
	3.4000(6)	2.7727(9)	2.8686(6)	2.9829(8)	2.7914(8)	2.8068(6)	2.7777(6)	2.7205(6)
M-Cl(Br)	2.3810(8)	2.5229(14)	2.4436(9)	2.2432(11)	2.2095(13)	2.3715(5)	2.2238(7)	2.3550(6)
	2.3433(9)	2.5143(15)	2.4442(9)					
		2.4989(15)	2.4927(9)					
M-$S_{(a)}$	2.4270(8)	2.3341(14)	2.2951(9)	2.3174(7)	2.2456(8)	2.2563(7)	2.2146(8)	2.2073(10)
	2.3885(8)	2.3278(14)	2.2963(9)	2.3174(7)	2.2456(8)	2.2561(7)	2.2172(7)	2.2139(10)
	2.2799(9)	2.3303(14)	2.2820(10)	2.3122(11)	2.2457(12)	2.2513(7)	2.2191(7)	2.2073(10)
av. Mo-Mo	2.8104	2.9299	2.8873	2.8397	2.8657	2.8716	2.8478	2.8408
av. Mo-$S_{(a)}$ (Mo_2M face)	2.3778	2.3278	2.3284	2.3630	2.3444	2.3484	2.3371	2.3309
av. Mo-$S_{(b)}$ (Mo_3 face)	2.3393	2.3498	2.3484	2.3303	2.3305	2.3350	2.3439	2.3346

allow only a cautious comparison. For example, some distances do not follow the the proposed trend, *e.g.* the reletively short Mo-V distances in chloride-bridged $[Mo_3S_4V]$ dimer **3** and the relatively long Mo-Mn and Mn-S distances in $[Mo_3S_4Mn]$ cluster **5**, the latter of which are possibly due to the presence of a high-spin Mn(II) center. The Mo-$S_{(a)}$ distances on the triangular Mo_2M faces seem to correlate with the Mo-M distances, possibly because the strong Mo-M interactions can bring Mo closer to $S_{(a)}$. On the other hand, the Mo-$S_{(b)}$ distances on the Mo_3 faces are nearly constant across **2**-**8**. The coordination number of M should affect the Mo-M, M-Cl(Br), and M-S distances, even though we were not able to find clear correlations.

As the $[Mo_3S_4M]$ cores contain Mo-M and Mo-Mo interactions, an estimation of the oxidation state of M is not straightforward. Nevertheless, the M-Cl(Br) distances in **2**-**8** provide some clues. The five-coordinate Ti center in **2** adopts a square-pyramidal geometry, with a sulfur atom at the apical position and two chloride atoms on the basal positions. The mean Ti-Cl distance of 2.3622(9) Å is comparable to that of the Ti(III) complex ([12]aneP_3Et_3)$TiCl_3$ (2.353(4) Å; [12]aneP_3Et_3 = 1,5,9-triethyl-1,5,9-triphosphacyclododecane),[19] but shorter than that of the Ti(II) complex $TiCl_2$(dmpe)$_2$ (2.440(4) Å; dmpe = 1,2-bis(dimethylposphino)ethane).[20] On the other hand, the average M-(μ-Cl) distances in $[Mo_3S_4M]$ dimers **3** (M = V; 2.5120(15) Å) and **4** (M = Cr; 2.4603(9) Å) render assignments of their oxidation states difficult, as they are somewhat longer than those in structurally analogous M(μ-Cl)$_3$M complexes of V(II/III) and Cr(II/III), *e.g.* 2.477(1) Å for the V(II) complex $[(THF)_3V(\mu\text{-}Cl)_3V(THF)_3]_2[Zn_2Cl_6]$,[21] 2.472(2) Å for the V(III) compmlex $[NEt_4]_3[Cl_3V(\mu\text{-}Cl)_3VCl_3]$,[22] 2.364(3) Å for the Cr(II) complex [Cp*Cr(μ-Cl)$_3$CrCp*][$BMe_2(C_6F_5)_2$],[23] and 2.408(3) Å for the Cr(III) complex $[NEt_3H]_3[Cl_3Cr(\mu\text{-}Cl)_3CrCl_3]$.[24] The Mn(II) state of **5** is reflected in its Mn-Cl distance (2.2432(11) Å), which is slightly shorter but still comparable to that of the Mn(II) complex $Tm^{Dip}MnCl$ (2.295(4) Å; Tm^{Dip} = hydrotris(mercaptoidazolyl)borate with 2,6-$^{i}Pr_2C_6H_3$ (Dip) substituents),[25] in which the Mn(II) center adopts a tetrahedral $Mn(S)_3Cl$ coordination environment. Similarly, the Fe-Cl distance in **6a** (2.2095(13) Å) is comparable to that of the Fe(II) complex $Tm^{Dip}FeCl$ (2.2381(6) Å).[25] The Fe-X distances in **6a** (2.2095(13) Å) and **6b** (2.3715(5) Å) are also analogous to those in cubic $[Mo_3S_4Fe]$ clusters $Tp_3Mo_3S_4FeX$ (X = Cl: 2.235(4) Å; X = Br: 2.334(4) Å; Tp = hydrotris(pyrazolyl)borate),[26] which have been assigned as the $Mo(IV)Mo(III)_2Fe(II)$ state. An Fe(II) state was further supported by the Mössbauer spectrum and the theoretical analysis of **6a** as discussed below (*vide infra*). For **7** and **8**, Co(II) and Ni(II) states were proposed based on a comparison of the Co-Cl distance between **7** (2.2238(7) Å) and $Tm^{Dip}CoCl$ (2.242(2) Å)[25] as well as the Ni-Br distance between **8** (2.3550(6) Å) and $^{Cl}Tm^{tBu}NiBr$ (2.3660(17) Å; ^{Cl}Tm = chlorotris(mercaptoidazolyl)borate)[27]. Even though these M-Cl(Br) distances give some indications on the oxidation states of M, an assessment based exclusively on structural data is not unequivocal. Further spectroscopic analyses, such as X-ray emission spectroscopy (XES),[28] would be required for clarification. In this context, it should be noted that a detailed analysis was conducted for $[Mo_3S_4Fe]$ cluster **6a** on the basis of its ^{57}Fe Mössbauer spectrum and DFT calculations (*vide infra*).

Redox Properties of Cubic Clusters 2, 3, and 5-8.

Given the various redox functions that have been demonstrated for biological and synthetic cubane-type clusters, the electrochemical properties of cubane-type clusters **2**, **3**, and **5**-**8** were investigated (the yield of $[Mo_3S_4Cr]$ dimer **4** was too low for such an investigation). Table 2 summarizes the redox potentials of reversible processes and the rest potentials (vs. $Cp_2Fe/[Cp_2Fe]^+$) observed in the cyclic voltammograms, which are shown in the supporting information (Figures S6-S12). The redox properties of **2**, **3**, and **5**-**8** exhibit no systematic trend, which supports that the $[Cp^*_3Mo_3S_4]$ platform is not a simple metallo-ligand, but the presence of various electronic

Table 2 Electrochemical Data for Cubic Clusters (potentials in V relative to $Cp_2Fe/[Cp_2Fe]^+$).

	2	**3**	**5**	**6a**	**6b**	**7**	**8**
M	Ti	V	Mn	Fe	Fe	Co	Ni
rest potential	–0.75	–0.91	–1.08	–0.63	–0.66	–0.85	–0.93
1st reduction $E_{1/2}$	–1.34	–1.33	–1.73			–1.74	
1st oxidation $E_{1/2}$	–0.28	–0.35		–0.52	–0.48	–0.75	–0.27
2nd oxidation $E_{1/2}$		–0.06					

interactions among the four metal centers within the $[Mo_3S_4M]$ cubes.

The $[Mo_3S_4Ti]$ cube **2** exhibited reversible oxidation and reduction processes at $E_{1/2}$ = –0.28 V and –1.34 V, in addition to irreversible reduction waves at E_{pc} = –1.67 and –2.17 V. A weak feature appeared at around –0.8 V after scanning at $E_{1/2}$ = –0.28 V, which suggests a partial decomposition due to instability of the 1e-oxidized species $[\mathbf{2}]^+$. The $[Mo_3S_4V]$ dimer **3** showed multiple waves in its cyclic voltammogram. Two reversible oxidation processes appeared at $E_{1/2}$ = –0.35 and –0.06 V, while a reversible reduction process was observed at $E_{1/2}$ = –1.33 V. An irreversible anodic feature appeared around the rest potential at E_{pa} = –0.99 V, which was found after scanning the reversible process at $E_{1/2}$ = –1.33 V. This suggests that the 1e-reduced form of **3** is unstable under the applied conditions. Scanning to the negative region beyond –1.33 V led to the appearance of an irreversible wave at E_{pc} = –1.63 V and a reversible wave at $E_{1/2}$ = –1.89 V. We tentatively assigned the feature at $E_{1/2}$ = –1.89 V to a redox couple of the monomeric $[Mo_3S_4V]$ cube, given that its electronic current is approximately twice of that for the process at $E_{1/2}$ = –1.33 V. The feature at E_{pc} = –1.63 V may be followed by a split of the $[Mo_3S_4V]$ dimer into two monomers, which may lead to the appearance of an irreversible process. The $[Mo_3S_4Mn]$ cube **5** exhibited a reversible reduction process at $E_{1/2}$ = –1.73 V, while scanning toward the positive region revealed complicated features, probably due to degradation. The cyclic voltammograms of $[Mo_3S_4Fe]$ cubes **6a** and **6b** are similar and exhibit a reversible oxidation process at $E_{1/2}$ = –0.52 V (**6a**) and –0.48 V (**6b**). These oxidation potentials are significantly more negative than the corresponding potential of the related cluster $Tp_3Mo_3S_4FeCl$ ($E_{1/2}$ = +0.52 V vs SCE),[26] suggesting that the electron-donating properties of Cp* are stronger than that of Tp. Further scanning toward the positive region showed an irreversible wave at E_{pa} = +0.61 V (**6a**) and +0.65 V (**6b**), as well as a quasi-reversible process at $E_{1/2}$ = +0.75 V (**6a**) and +0.76 V (**6b**). After scanning this region, a weak cathodic feature appeared at E_{pc} = –1.36 V (**6a**) and –1.38 V (**6b**). The $[Mo_3S_4Co]$ cube **7** showed one reversible oxidation and one reversible reduction processes at $E_{1/2}$ = –0.75 V and –1.74 V, respectively. In a manner analogous to **6a** and **6b**, an irreversible wave and a quasi-reversible process also appeared in the cyclic voltammogram of **7** at +0.64 V and +0.75 V, respectively. However, scanning in this region leads to significant degradation of **7**, which results in the appearance of complicated features. The $[Mo_3S_4Ni]$ cube **8** exhibited a reversible oxidation process at $E_{1/2}$ = –0.27 V. Scanning toward the positive region at around +0.8 V led to partial degradation and the appearance of irreversible cathodic peaks at E_{pc} = –1.39 V and –1.98 V.

A feature common in most of the cyclic voltammograms of cubic clusters is the appearance of an anodic wave at around +0.7 V, which we have tentatively attributed to the $[Cp^*_3Mo_3S_4]^{+/2+}$ process, based on the observation of the corresponding redox process in Figure 2 (blue trace). Under oxidizing conditions, we thus propose that a part of the cubic cluster dissociates the hetero-metal M to generate the cationic Mo_3 species $[Cp^*_3Mo_3S_4]^+$. This notion is consistent with the electro-spray ionization mass spectra (ESI-MS) of **2**, **3**, **6b**, and **8** in THF (Figures S13-S16), which revealed signals for $[cluster]^+$ and $[Cp^*_3Mo_3S_4]^+$. This hypothesis is further supported by the ready decomposition of cubic clusters upon exposure to air, which affords the greenish color that is characteristic for the $[Cp^*_3Mo_3S_4]$ platform.

^{57}Fe Mössbauer Spectrum and Theoretical Analysis of the $[Mo_3S_4Fe]$ Cluster 6a.

In order to further assess the electronic structure of Fe in the $[Mo_3S_4Fe]$ cluster **6a**, the ^{57}Fe Mössbauer spectrum was measured at 78 K on a crystalline sample at zero-field, yielding a doublet at an isomer shift (IS) of 0.563(3) mm/s with a small quadrupole split (QS) of 0.266(5) mm/s (Figure 4). This IS value suggests a high-spin Fe(II) state,[29] which is in agreement with the pseudo-tetreahedral $Fe(S)_3Cl$ coordination environment. The small QS value is indicative of a relatively symmetric distribution of electron density around the Fe center in the $Fe(S)_3Cl$ coordination environment.

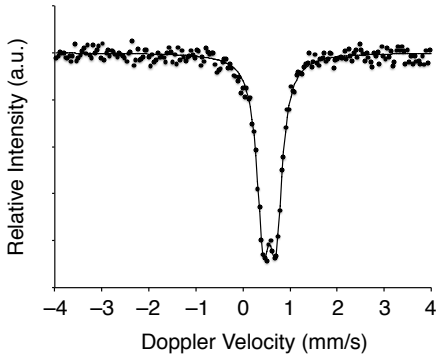

Figure 4 ^{57}Fe Mössbauer spectrum of **6a** at zero field and 78 K. The Doppler velocity scale was calibrated using the room-temperature Mössbauer spectrum of metallic iron foil.

The *S* = 0, 1, and 2 states of **6a** were fully optimized using the B3LYP-D3BJ and BP86-D3BJ functionals (Tables S4). Both density funcationls yield the *S* = 1 state as the ground state. The theoretically predicted *S* = 1 ground state is in agreement with the experimental magnetic moment of **6a** (2.4 μ_B at 295 K in CD_2Cl_2), which was determined by the Evans method. The Mössbauer parameters were calculated for both the X-ray and the optimized structures in the *S* = 0, 1, and 2 states using the TPSSh functional (Table S5). The calculated IS values of the three spin states of the X-ray structure (0.45-0.48 mm/s) are comparable and qualitatively in agreement with the experimental result (0.563(3) mm/s). On the other hand, the calculated QS values vary by the spin states, *i.e.,* 0.10 (*S* = 0), 0.21 (*S* = 1), and 1.08 (*S* = 2), revealing the *S* = 1 state as the best agreement. Similarly, the Mössbauer parameters calculated for the DFT-optimized structures in the *S* = 0, 1, and 2 states reveal relatively small differences for the IS values (0.26-0.43 mm/s) and significant differences for the QS values (0.20-3.65 mm/s), and those of the *S* = 1 state (IS = 0.36 mm/s and QS = 0.20 mms/) agree closest with the experimental results. It should be noted that the QS value is more sensitive to the coordination environment of the metal than the IS value. The *S* = 1 state, which shows the best agreement with the QS value, seems to be the most reasonable assignment under the applied experimental conditions.

Conclusions

In this study, we have demonstrated that the charge of the anionic Mo_3 cluster $[Cp^*_3Mo_3S_4]^-$ [**1**]$^-$ modifies the versatility of the platform. The anionic $[Cp^*_3Mo_3S_4]^-$ platform successfully accommodates halides of first-row transition metals from group 4-10 (M) to furnish a series of $[Mo_3S_4M]$ cubes through salt-metathesis-type reactions. This stands in contrast to the cationic $[Cp^*_3Mo_3S_4]^+$ platform, which is inert toward early transition-metal halides. The resulting $[Mo_3S_4M]$ cubes were structurally characterized, and their redox properties were investigated. The M:halide ratio for the $[Mo_3S_4M]$ cubes gradually icreases from 1:2 (Ti) to 1:1 (Mn, Fe, Co, and Ni), exhibiting a higher tendency of early transition metals to tolerate high oxidation states and larger ionic radii. As a wide range of metals are compatible with the anionic $[Cp^*_3Mo_3S_4]^-$ platform, one can apply the present synthetic protocol for $[Mo_3S_4M]$ cubes to various second- and third-row transition metals in order to generate a number of prospective catalysts for homogeneous reactions, even though the cationic $[Cp^*_3Mo_3S_4]^+$ platform is already able to accommodate some late transition metals from the second-row such as Ru and Pd.[8,9] Recent studies have demonstrated the potential of cubic metal-sulfur clusters for the activation of small molecules,[6,16] and therefore, such $[Mo_3S_4M]$ cubes can potentially be employed in the stoichiometric/catalytic reduction of N_2, CO_2, or CO. Research in this direction is currently in progress in our group, and the results will be reported in due course. One could possibly also apply the present $[Mo_3S_4M]$ cubes as catalyst precursors to various homogeneous processes.

Experimental Section

General Procedures

All reactions were carried out under an atmosphere of N_2 or Ar using either Schlenk-line or glovebox techniques. Hexane, toluene, THF, and CH_2Cl_2 were purified by passing over columns of activated alumina and a supported copper catalyst supplied by Hansen & Co. Ltd. Deuterated solvents were dried and vacuum-transferred prior to use. ^{1}H NMR spectra were recorded on JEOL JNM ECS600 or ECS500 spectrometers. UV-vis spectra were measured on a JASCO V770 spectrometer. Elemental analyses were carried out on powdered crystalline samples sealed in tin capsules under N_2, using an Elementar Analytical vario MICRO cube elemental analyzer. Cyclic voltammograms were measured in a single-compartment cell under a N_2 atmosphere at room temperature using a BAS ALS-660A electrochemical analyzer. The supporting electrolyte, 0.2 M tetrabutylammonium hexafluorophosphate ($[^nBu_4N][PF_6]$), was recrystallized from THF prior to use. All potentials are referenced to $Cp_2Fe/[Cp_2Fe]^+$. Mössbauer measurements were performed in a conventional transmission mode on a Mössbauer spectrometer (Topologic Systems Co. Model-222) using a ^{57}Co(Rh) source (925 MBq). The spectral curve fitting was conducted out by using MossWinn 4.0Pre on the assumption of the sum of the Lorentzian curves. The Doppler velocity scale was calibrated with respect to α-iron at room temperature, and the isomer shifts are given relative to α-iron. Low-temperature experiments were carried out in a glovebox using a Techno Sigma UCR-150-GB. $Cp^*_3Mo_3S_4$ (**1**) was synthesized on a gram scale according to a reported procedure.[16] All other chemicals were purchased from common commercial sources and used without further purification.

[K(18-crown-6)][$Cp^*_3Mo_3S_4$], [K(18-crown-6)][1]$^-$. $Cp^*_3Mo_3S_4$ (0.200 g, 0.243 mmol) was dissolved in THF (10 mL), and 18-crown-6 (66 mg, 0.250 mmol) was added. This solution was cooled to –100 °C before KC_8 (33 mg, 0.244 mmol) was added. The resulting mixture was stirred and gradually warmed to room temperature to lead to a slight color change from green to yellowish green. After stirring overnight, the mixture was filtered through a disposable filter (Whatman 25 mm) to obtain a green solution that was cooled to –30 °C to afford dark green blocks of **1** (153 mg, 0.136 mmol, 56% yield). ^{1}H NMR (THF-$[D]_8$, r.t.): δ 13.3 ($w_{1/2}$ = 44 Hz, Cp*), 3.64 (18-crown-6). Solution magnetic moment (THF-$[D]_8$, 297 K): μ_{eff} = 2.3 μ_B. Cyclic Voltammetry (THF): $E_{1/2}$ = –0.21 V, –1.00 V, –2.50 V. UV-vis (THF): λ_{max} = 381 nm (6400 cm^{-1}M^{-1}), 671 nm (1600 cm^{-1}M^{-1}). Anal. Calcd for $C_{42}H_{69}KMo_3O_6S_4$: C, 44.83; H, 6.18; S, 11.40. Found: C, 45.22; H, 6.08; S, 11.19.

$Cp^*_3Mo_3S_4TiCl_2$ (2).[16] A THF solution of $Na(C_{10}H_8)$ (19.5 mM, 62 mL, 1.21 mmol) was added to a THF (30 mL) solution of $Cp^*_3Mo_3S_4$ (1.00 g, 1.22 mmol) at –100 °C. The solution was stirred and gradually warmed to room temperature, which led to a color change from green to brownish green. The mixture was cooled to –100 °C, before $TiCl_3(THF)_3$ (451 mg, 1.22 mmol) was added. The resulting mixture was warmed to room temperature, and stirring was continued for 5 days to give a dark brown suspension. The mixture was concentrated under reduced pressure to *ca.* 5 mL, and then cooled to –30 °C to cause precipitation. The supernatant was removed, and the resulting dark brown solid was washed with hexane (2 x 20 mL) and dried. The residue was dissolved in CH_2Cl_2 (18 mL), and hexane (*ca.* 100 mL) was carefully layered on top of this solution. Slow diffusion between the two layers resulted in the formation of brown plates of **2**·CH_2Cl_2, which were washed with hexane (2 x 15 mL) and dried under reduced pressure. The crystals were suspended in THF (15 mL) and stirred overnight at room temperature. Evaporation of THF and CH_2Cl_2 furnished solvent-free **2** (801 mg, 0.854 mmol, 70%) as a brown powder. ^{1}H NMR (CD_2Cl_2, r.t.): δ 9.23 ($w_{1/2}$ = 8 Hz, Cp*). Solution

magnetic moment (CD_2Cl_2, 297 K): μ_{eff} = 1.3 μ_B. Cyclic Voltammetry (CH_2Cl_2): $E_{1/2}$ = –0.28 V, –1.34 V. UV-vis (CH_2Cl_2): λ_{max} = 415 nm (sh, 1200 $cm^{-1}M^{-1}$), 753 nm (660 $cm^{-1}M^{-1}$). Anal. calcd. for $C_{30}H_{45}Cl_2Mo_3S_4Ti$: C, 38.31; H, 4.82; S, 13.64. Found: C, 38.77; H, 4.70; S, 13.24.

$[Cp^*_3Mo_3S_4V]_2(\mu\text{-}Cl)_3$ (3). In a manner similar to the synthesis of **2**, $Cp^*_3Mo_3S_4$ (1.00 g, 1.22 mmol) in THF (30 mL) was treated with $Na(C_{10}H_8)$ (19.5 mM in THF, 62 mL, 1.21 mmol). $VCl_3(THF)_3$ (455 mg, 1.22 mmol) was added to this solution at –100 °C, and the mixture was gradually warmed to room temperature. Stirring was continued for 5 days, affording a dark brown suspension. After concentration to *ca*. 5 mL, the mixture was cooled to –30 °C to cause precipitation. The supernatant was removed, and the resulting dark brown solid was washed with hexane (2 x 20 mL) and dried. The residue was dissolved in CH_2Cl_2 (20 mL), and hexane was layered on top of this solution. Slow diffusion between the two layers resulted in the formation of brown plates of **3**, which were washed with hexane (2 x 15 mL) and dried. THF (15 mL) was added, and the resulting suspension was stirred overnight and again dried under reduced pressure to afford a brown powder of **3** (574 mg, 0.311 mmol, 51% yield). Crystals used for X-ray crystallography contained adventitious anthracene and acetonitrile, which were severely disordered and thus treated as a diffuse contribution without specific atom positions. ^{1}H NMR (CD_2Cl_2, r.t.): δ 4.90 ($w_{1/2}$ = 3 Hz, Cp*). Solution magnetic moment (CD_2Cl_2, 297 K): μ_{eff} = 2.4 μ_B. Cyclic Voltammetry (CH_2Cl_2): $E_{1/2}$ = –0.06 V, –0.35 V, –1.33 V. UV-vis (CH_2Cl_2): λ_{max} = 560 nm (4200 $cm^{-1}M^{-1}$). Anal. Calcd. for $C_{60}H_{90}Cl_3Mo_3S_4V_2$: C, 38.92; H, 4.90; S, 13.85. Found: C, 39.12; H, 5.07; S, 13.44.

Formation of a trace amount of $[Cp^*_3Mo_3S_4Cr]_2(\mu\text{-}Cl)_3$ (4). In a manner similar to the synthesis of **2**, $Cp^*_3Mo_3S_4$ (0.300 g, 0.365 mmol) in THF (10 mL) was treated with $Na(C_{10}H_8)$ (19.5 mM in THF, 9 mL, 0.175 mmol). $CrCl_2$ (44 mg, 0.358 mmol) was added to this solution at –100 °C, and the mixture was gradually warmed to room temperature. Stirring was continued for 2 days, which afforded a brown suspension. After concentration to *ca*. 2 mL, the mixture was cooled to –30 °C in order to cause precipitation. The supernatant was removed, and the residue was dissolved in CH_2Cl_2 (2 mL) before hexane was layered on top of this solution. Slow diffusion between the two layers resulted in the formation of a trace amount of brownish red plates of **4**·$(CH_2Cl_2)_2$·$(hexane)_2$. This compound was characterized only by X-ray crystallography.

$Cp^*_3Mo_3S_4MnCl$ (5). In a manner similar to the synthesis of **2**, $Cp^*_3Mo_3S_4$ (0.300 g, 0.365 mmol) in THF (10 mL) was treated with $Na(C_{10}H_8)$ (19.5 mM in THF, 18.5 mL, 0.358 mmol). $MnCl_2$ (45 mg, 0.358 mmol) was added to this solution at –100 °C, and the mixture was gradually warmed to room temperature. Stirring was continued for 4 days, giving a greenish brown suspension. The mixture was cooled to –30 °C to cause precipitation, and the supernatant was removed. After washing with hexane (2 x 20 mL), the residue was dissolved in CH_2Cl_2 (6 mL), and hexane was layered on top of this solution. Slow diffusion between the two layers resulted in the formation of dark brown plates of **5** (35 mg, 0.040 mmol, 11% yield). A crystallographic analysis was carried out with crystals of **5**·1/2(THF) obtained from a THF solution. ^{1}H NMR (CD_2Cl_2, r.t.): δ –0.01 ($w_{1/2}$ = 24 Hz, Cp*). Solution magnetic moment (CD_2Cl_2, 297 K): μ_{eff} = 3.9 μ_B. Cyclic Voltammetry (CH_2Cl_2): $E_{1/2}$ = –0.01 V. UV-vis (CH_2Cl_2): λ_{max} = 530 nm (910 $cm^{-1}M^{-1}$), 635 nm (820 $cm^{-1}M^{-1}$). Anal. Calcd. for $C_{30}H_{45}ClMnMo_3S_4$: C, 39.50; H, 4.97; S, 14.06. Found: C, 39.03; H, 5.21; S, 14.35.

$Cp^*_3Mo_3S_4FeCl$ (6a). In a manner similar to the synthesis of **2**, $Cp^*_3Mo_3S_4$ (1.02 g, 1.24 mmol) in THF (30 mL) was treated with $Na(C_{10}H_8)$ (19.5 mM in THF, 63 mL, 1.22 mmol). $FeCl_2$ (163 mg, 1.29 mmol) was added to this solution at –100 °C, and the mixture was gradually warmed to room temperature. Stirring was continued overnight, giving a dark reddish purple suspension. After concentration to *ca*. 5 mL, the mixture was cooled to –30 °C to cause precipitation. The supernatant was removed, and the resulting dark brown solid was washed with hexane (10 mL) and dried. The residue was dissolved in CH_2Cl_2 (15 mL), and hexane was layered on top of this solution. Slow diffusion between the two layers resulted in the formation of reddish purple sticks of **6a**·CH_2Cl_2, which were washed with hexane (2 x 10 mL) and dried. THF (15 mL) was added, and the resulting suspension was stirred overnight and again dried under reduced pressure to afford a reddish purple powder of **6a** (750 mg, 0.820 mmol, 66% yield). ^{1}H NMR (CD_2Cl_2, r.t.): δ –1.23 ($w_{1/2}$ = 710 Hz, Cp*). Solution magnetic moment (CD_2Cl_2, 295 K): μ_{eff} = 2.4 μ_B. Cyclic Voltammetry (CH_2Cl_2): $E_{1/2}$ = –0.52 V. UV-vis (CH_2Cl_2): λ_{max} = 510 nm (1900 $cm^{-1}M^{-1}$), 635 nm (710 $cm^{-1}M^{-1}$). Mössbauer spectrum (78 K, zero-field): IS = 0.563(3) mm/s, QS = 0.266(5) mm/s, LW = 0.326(8) mm/s. Anal. Calcd. for $C_{30}H_{45}ClFeMo_3S_4$: C, 39.46; H, 4.97; S, 14.05. Found: C, 39.85; H, 4.98; S, 13.37. See the note below for unsuccessful elemental analysis.

$Cp^*_3Mo_3S_4FeBr$ (6b). In a manner similar to the synthesis of **2**, $Cp^*_3Mo_3S_4$ (1.00 g, 1.22 mmol) in THF (30 mL) was treated with $Na(C_{10}H_8)$ (19.5 mM in THF, 62 mL, 1.21 mmol). $FeBr_2$ (262 mg, 1.21 mmol) was added to this solution at –100 °C, and the mixture was gradually warmed to room temperature. Stirring was continued overnight, giving a dark red suspension. After concentration to *ca*. 5 mL, the mixture was cooled to –30 °C to cause precipitation. The supernatant was removed, and the resulting dark red solid was washed with hexane (2 x 20 mL) and dried. The residue was dissolved in CH_2Cl_2 (14 mL), and hexane was layered on top of this solution. Slow diffusion between the two layers resulted in the formation of red sticks of **6b**, which were washed with hexane (2 x 15 mL) and dried. THF (15 mL) was added, and the resulting suspension was stirred overnight and again dried under reduced pressure to afford a red powder of **6b** (784 mg, 0.817 mmol, 67% yield). ^{1}H NMR (CD_2Cl_2, r.t.): δ –0.96 ($w_{1/2}$ = 92 Hz, Cp*). Solution magnetic moment (CD_2Cl_2, 297 K): μ_{eff} = 2.4 μ_B. Cyclic Voltammetry (CH_2Cl_2): $E_{1/2}$ = –0.48 V. UV-vis (CH_2Cl_2): λ_{max} = 513 nm (2000 $cm^{-1}M^{-1}$), 640 nm (690 $cm^{-1}M^{-1}$). Anal. Calcd. for $C_{30}H_{45}BrFeMo_3S_4$: C, 37.63; H, 4.74; S, 13.40. Found: C, 37.34; H, 4.76; S, 13.01.

$Cp^*_3Mo_3S_4CoCl$ (7). *Method A, from a mixture of $Cp^*_3Mo_3S_4$ and $Na(C_{10}H_8)$*: In a manner similar to the synthesis of **2**, $Cp^*_3Mo_3S_4$ (0.500 g, 0.608 mmol) in THF (15 mL) was treated with $Na(C_{10}H_8)$ (19.5 mM in THF, 31 mL, 0.605 mmol). $CoCl_2$ (79 mg, 0.609 mmol) was added to this solution at –100 °C, and the mixture was gradually warmed to room temperature. Stirring was continued overnight, giving a dark brown suspension. After concentration to *ca*. 10 mL, the mixture was cooled to –30 °C to cause precipitation. The supernatant was removed, and the resulting dark brown solid was washed with hexane (2 x 15 mL) and dried. The residue was dissolved in CH_2Cl_2 (8 mL), and hexane was layered on top of this solution. Slow diffusion between two layers resulted in the formation of dark brown blocks of **7**·CH_2Cl_2. THF (10 mL) was added, and the resulting suspension was stirred overnight and again dried under reduced pressure to afford a dark brown powder of **7** (367 mg, 0.401 mmol, 66% yield). *Method B, from [K(18-crown-6)][**1**]*$^-$: [K(18-crown-6)][$Cp^*_3Mo_3S_4$]·$(THF)_3$ (350 mg, 0.261 mmol) was treated with $CoCl_2$ (34 mg, 0.262 mmol) in THF (20 mL). Dark brown blocks of **7**·CH_2Cl_2 (179 mg, 0.179 mmol, 69% yield) were obtained after the workup. ^{1}H NMR (CD_2Cl_2, r.t.): δ 2.27 ($w_{1/2}$ = 5 Hz, Cp*). Solution magnetic moment (CD_2Cl_2, 297 K): μ_{eff} = 1.8 μ_B. Cyclic Voltammetry (CH_2Cl_2): $E_{1/2}$ = –0.75 V, –1.74 V. UV-vis (CH_2Cl_2): λ_{max} = 460 nm (3000 $cm^{-1}M^{-1}$), 649 nm (810 $cm^{-1}M^{-1}$). Anal. Calcd. for $C_{30}H_{45}ClCoMo_3S_4$: C, 39.33; H, 4.95; S, 14.00. Found: C, 39.15; H, 5.37; S, 12.32. See the note below for unsuccessful elemental analysis.

$Cp^*_3Mo_3S_4NiBr$ (8). In a manner similar to the synthesis of **2**, $Cp^*_3Mo_3S_4$ (1.00 g, 1.22 mmol) in THF (30 mL) was treated with $Na(C_{10}H_8)$ (19.5 mM in THF, 62 mL, 0.605 mmol). $NiBr_2$(DME) (376 mg, 1.22 mmol) was added to this solution at –100 °C, and the mixture was gradually warmed to room temperature. Stirring was continued overnight, giving a red suspension. After concentration to *ca*. 40 mL, the mixture was cooled to –30 °C to cause precipitation. The supernatant was removed, and the resulting dark brown solid was washed with hexane (2 x 20 mL) and dried. The residue was dissolved in CH_2Cl_2 (17 mL), and hexane was layered on top of this solution. Slow diffusion between the two layers resulted in the formation of dark brown blocks of **8**·$(CH_2Cl_2)_2$. THF (10 mL) was added, and the resulting suspension was stirred for overnight and again dried under reduced pressure to afford a dark brown powder of **8** (675 mg, 0.708 mmol, 58% yield). ^{1}H NMR (CD_2Cl_2, r.t.): δ 1.96 ($w_{1/2}$ = 2 Hz, Cp*). Solution magnetic moment (CD_2Cl_2, 297 K): μ_{eff} = 2.4 μ_B. Cyclic Voltammetry (CH_2Cl_2): $E_{1/2}$ = –0.27 V. UV-vis (CH_2Cl_2): λ_{max} = 393 nm (5800 $cm^{-1}M^{-1}$). Anal. Calcd. for $C_{30}H_{45}BrMo_3NiS_4$: C, 37.52; H, 4.72; S, 13.36. Found: C, 37.90; H, 4.78; S, 13.21.

Unsuccessful Elemental Analyses for Some Cubane-Type Clusters. We have been unable to obtain satisfactory elemental analysis values for clusters **6a** and **7**. Even though several attempts have been made, fine powders **6a** and **7** obtained after removal of CH_2Cl_2 from **6a**·CH_2Cl_2 and **7**·CH_2Cl_2 afforded low sulfur values, which are possibly due to incomplete combustion or thermal degradation. However, we cannot rule out the possibility of contamination definitively. The addition of a combustion accelerator (WO_3 powder) did not improve the results. Regardless, various measurements indicated sufficient purity of these compounds.

Computataional methods. All structures were optimized without any constrains using the ORCA 2.9 program.[30] The scalar relativistic effects with the ZORA Hamiltonian were employed.[31] The dispersion-corrected BP86[32] functional, including dispersion corrections,[33] was used for structure optimizations. The ZORA-recontracted[34] TZVP and def2-TZVP basis sets,[35] as well as the decontracted def2-TZVP/J auxiliary basis set for the Coulomb density fitting approximation were employed. Final potential energies of the optimized structures were calculated from the dispersion corrected B3LYP[36] functional with dispersion corrections,[33] employing the above basis sets. Increased integration grids (Grid6) and tight SCF criteria were applied for all calculations. The Mössbauer parameters, *i.e.,* the isomer-shift (δ or IS) and the quadrupole splitting (ΔE_Q or QS), were calculated using the TPSSh funcational[37] with CP(PPP) basis sets for Fe,[38] while the TZVP[39] functional was used for the remaining atoms. For the isomer-shift calculations, the following values were used: α = -0.376, β = 4.130, and C = 11810.[40] Molecular orbital pictures and spin-density plotes were generated starting from the optimized structures, while single-point energy calculations were carried out using the Gaussian16 program.[41] The B3LYP-D3BJ funcational and SDD[42] basis sets as well as associated effective core potentials were used for Fe and Mo, while the def2TZVP[43] basis set was used for other atoms.

Acknowledgements

This work was financially supported by the PRESTO program of the Japan Science and Technology Agency (JPMJPR1342), Grant-in-Aids for Scientific Research (16H04116 and 18H04246) from the Japanese Ministry of Education, Culture, Sports, Science and Technology (MEXT), the Hori Sciences and Arts Foundation, and the Takeda Science Foundation. We are grateful to Prof. K. Tatsumi for providing access to instruments, to Prof. S. Muratsugu for generous advice on electrochemical measurements, and to Prof. R. E. Cramer for his help in crystallographic analysis. Super-computing resources at the Institute of Molecular Science in Japan are also acknowledged.

Keywords: Molybdenum • Sulfur • Cubane • Clusters • First-row transition metals

[1] a) S. C. Lee, W. Lo, R. H. Holm, *Chem. Rev.* **2014**, *114*, 3579-3600; b) J. Liu, S. Chakraborty, P. Hosseinzadeh, Y. Yu, S. Tian, I. Petrik, A. Bhagi, Y. Lu, *Chem. Rev.* **2014**, *114*, 4366-4469; c) S. Ohta, Y. Ohki, *Coord. Chem. Rev.* **2017**, *338*, 207-225.

[2] a) H. Ogino, S. Inomata, H. Tobita, *Chem. Rev.* **1998**, *98*, 2093-2121; b) M. Hidai, S. Kuwata, Y. Mizobe, *Acc. Chem. Res.* **2000**, *33*, 46-52.

[3] H. Seino, M. Hidai, *Chem. Sci.* **2011**, *2*, 847-857.

[4] H. Beinert, M. C. Kennedy, C. D. Stout, *Chem. Rev.* **1996**, *96*, 2335-2373.

[5] W. Wang, E. Oldfield, *Angew. Chem. Int. Ed.* **2014**, *53*, 4294-4310.

[6] a) J. G. Rebelein, M. T. Stiebritz, C. C. Lee, Y. Hu, *Nat. Chem. Biol.* **2017**, *13*, 147-149; b) M. T. Stiebritz, C. J. Hiller, N. S. Sickerman, C. C. Lee, K. Tanifuji, Y. Ohki, Y. Hu, *Nat. Catal.* **2018**, *1*, 444-451.

[7] a) D. Coucouvanis, P. E. Mosier, K. D. Demadis, S. Patton, S. M. Malinak, C. G. Kim, M. A. Tyson, *J. Am. Chem. Soc.* **1993**, *115*, 12193-12194; b) L. J. Laughlin, D. Coucouvanis, *J. Am. Chem. Soc.* **1995**, *117*, 3118-3125; c) K. D. Demadis, S. M. Malinak, D. Coucouvanis, *Inorg. Chem.* **1996**, *35*, 4038-4046; d) D. Coucouvanis, K. D. Demadis, S. M. Malinak, P. E. Mosier, M. A. Tyson, L. J. Laughlin, *J. Mol. Catal. A* **1996**, *107*, 123-135; e) S. M. Malinak, A. M. Simenov, P. E. Mosier, C. E. McKenna, D. Coucouvanis, *J. Am. Chem. Soc.* **1997**, *119*, 1662-1667.

[8] a) K. Tanaka, Y. Imasaka, M. Tanaka, M. Honjo, T. Tanaka, *J. Am. Chem. Soc.* **1982**, *104*, 4258-4260; b) M. Tezuka, T. Yajima, A. Tsuchiya, Y. Matsumoto, Y. Uchida, M. Hidai, *J. Am. Chem. Soc.* **1982**, *104*, 6834-6836; c) M. Nakazawa, Y. Mizobe, Y. Matsumoto, Y. Uchida, M. Tezuka, M. Hidai, *Bull. Chem. Soc. Jpn.* **1986**, *59*, 809-814; d) K. Tanaka, M. Moriya, S. Uezumi, T. Tanaka, *Inorg. Chem.* **1988**, *27*, 137-143; e) K. Tanaka, R. Wakita, T. Tanaka, *J. Am. Chem. Soc.* **1989**, *111*, 2428-2433; f) K. Tanaka, T. Matsui, T. Tanaka, *J. Am. Chem. Soc.* **1989**, *111*, 3765-3767; g) N. Komeda, H. Nagao, T. Matsui, G. Adachi, K. Tanaka, *J. Am. Chem. Soc.* **1992**, *114*, 3625-3630.

[9] a) T. Murata, Y. Mizobe, H. Gao, Y. Ishii, T. Wakabayashi, F. Nakano, T. Tanase, S. Yano, M. Hidai, I. Echizen, H. Nanikawa, S. Motomura, *J. Am. Chem. Soc.* **1994**, *116*, 3389-3398; b) T. Wakabayashi, Y. Ishii, T. Murata, Y. Mizobe, M. Hidai, *Terahedron Lett.* **1995**, *36*, 5585-5588; c) T. Wakabayashi, Y. Ishii, K. Ishikawa, M. Hidai, *Angew. Chem. Int. Ed. Engl.* **1996**, *35*, 2123-2124; d) I. Takei, Y. Wakebe, K. Suzuki, Y. Enta, T. Suzuki, Y. Mizobe, M. Hidai, *Organometallics* **2003**, *22*, 4639-4641; e) I. Takei, Y. Enta, Y. Wakebe, T. Suzuki, M. Hidai, *Chem. Lett.* **2006**, *35*, 590-591.

[10] I. Takei, K. Dohki, K. Kobayashi, T. Suzuki, M. Hidai, *Inorg. Chem.* **2005**, *44*, 3768-3770.

[11] a) Y. Tao, B. Wang, B. Wang, L. Qu, J. Qu, *Org. Lett.* **2010**, *12*, 2726-2729; b) Y. Tao, B. Wang. J. Zhao, Y. Song, L. Qu, J. Qu, *J. Org. Chem.* **2012**, *77*, 2942-2946.

[12] a) M. Feliz, E. Guillamón, R. Llusar, C. Vincent, S. -E. Stirba, J. Pérez-Prieto, M. Barberis, *Chem. Eur. J.* **2006**, *12*, 1486-1492; b) E. Guillamón, R. Llusar, J. Pérez-Prieto, S. -E. Stiriba, *J. Organomet. Chem.* **2008**, *693*, 1723-1727.

[13] E. Pedrajas, I. Sorribes, E. Guillamón, K. Junge, M. Beller, R. Llusar, *Chem. Eur. J.* **2017**, *23*, 13205-13212.

[14] a) T. Shibahara, *Adv. Inorg. Chem.* **1991**, *37*, 143-173; b) M. Hidai, S. Kuwata, Y. Mizobe, *Acc. Chem. Res.* **2000**, *33*, 46-52; c) R. Llusar, S. Uriel, *Eur. J. Inorg. Chem.* **2003**, 1271-1290.

[15] a) B. Rink, M. Brorson, I. J. Scowen, *Organometallics* **1999**, *18*, 2309-2313; b) K. Herbst, M. Monari, M. Brorson, *Inorg. Chem.* **2001**, *40*, 2979-2985; c) I. Takei, K. Suzuki, Y. Enta, K. Dohki, T. Suzuki, Y. Mizobe, M. Hidai, *Organometallics* **2003**, *22*, 1790-1792

[16] Y. Ohki, K. Uchida, M. Tada, R. E. Cramer, T. Ogura, T. Ohta, *Nat. Commun.* **2018**, *9*, 3200.

[17] R. E. Cramer, K. Yamada, H. Kawaguchi, K. Tatsumi, *Inorg. Chem.* **1996**, *35*, 1743-1746.

[18] a) W. M. C. Sameera, J. E. McGrady *Dalton Trans*, **2008**, 6141-6149; b) M. Radon, *Phys.Chem.Chem.Phys.*, **2014**, *16*, 14479- 14488.

[19] R. J. Baker, P. C. Davies, P. G. Edwards, R. D. Farley, S. S. Liyanage, D. M. Murphy, B. Yong, *Eur. J. Inorg. Chem.* **2002**, 1975-1984.

[20] G. S. Girolami, G. Wilkinson, A. M. R. Galas, M. Thornton-Pett, M. B. Hursthouse, *J. Chem. Soc., Dalton Trans.* **1985**, 1339-1348.

[21] R. J. Bouma, J. H. Teuben, W. R. Beukema, R. L. Bansemer, J. C. Huffman, K. G. Caulton, *Inorg. Chem.* **1984**, *23*, 2715-2718.

[22] G. B. Karet, S. L. Castro, K. Folting, J. C. Bollinger, R. A. Heintz, G. Christou, *J. Chem. Soc., Dalton Trans.* **1998**, 67-72.

[23] P. Wei, D. W. Stephan, *Organometallics* **2003**, *22*, 1712-1717.

[24] P. W. Dyer, V. C. Gibson, J. C. Jeffery, *Polyhedron* **1995**, *14*, 3095-3098.

[25] S. Senda, Y. Ohki, T. Hirayama, D. Toda, J. -L. Chen, T. Matsumoto, H. Kawaguchi, K. Tatsumi, *Inorg. Chem.* **2006**, *45*, 9914-9925.

[26] T. Yamauchi, H. Takagi, T. Shibahara, H. Akashi, *Inorg. Chem.* **2006**, *45*, 5429-5437.

[27] K. Pang, J. M. Tanski, G. Parkin, *Chem. Commun.* **2008**, 1008-1010.

[28] a) C. J. Pollock, S. DeBeer, *Acc. Chem. Res.* **2015**, *48*, 2967-2975; b) J. K. Kowalska, A. W. Hahn, A. Albers, C. E. Schiewer, R. Bjornsson, F. A. Lima, F. Meyer, S. DeBeer, *Inorg. Chem.* **2016**, *55*, 4485-4497.

[29] a) P. Gütlich, E. Bill, A. X. Trautwein, *Mössbauer Spectroscopy and Transition Metal Chemistry, Fundamentals and Applications*, Springer, Heidelberg, **2011**, and references therein; b) R. E. Vandenberghe, E. De Grave, *Mössbauer Spectroscopy Tutorial Book* (Eds.: Y. Yoshida, G. Langouche), Springer, Heidelberg, **2013**, and references therein.

[30] F. Neese, *Wiley Interdiscip. Rev. Comput. Mol. Sci.*, **2012**, *2*, 73–78.

[31] a) E. van Lenthe, E. J. Baerends, J. G. Snijders, *J. Chem. Phys.*, **1993**, *99*, 4597–4610; b) E. van Lenthe, E. J. Baerends, J. G. Snijders, *J. Chem. Phys.*, **1994**, *101*, 9783–9792; c) C. van Wüllen, *J. Chem. Phys.*, **1998**, *109*, 392–399.

[32] a) J. P. Perdew, *Phys. Rev. B: Condens. Matter Mater. Phys.*, **1986**, *33*, 8822–8824; b) A. D. Becke, *Phys. Rev. A: At., Mol., Opt. Phys.*, **1988**, *38*, 3098–3100.

[33] S. Grimme, J. Antony, S. Ehrlich, H. Krieg, *J. Chem. Phys.*, **2010**, *132*, 154104–154119.

[34] D. A. Pantazis, X. Y. Chen, C. R. Landis, F. Neese, *J. Chem. Theory Comput.*, **2008**, *4*, 908–919.

[35] F. Weigend, R. Ahlrichs, *Phys. Chem. Chem. Phys.*, **2005**, *7*, 3297–3305.

[36] a) C. Lee, W. Yang, R. G. Parr, *Phys. Rev. B*, **1988**, *37*, 785-789; b) A. D. Becke, *J. Chem. Phys.* **1992**, *96*, 2155-2160; c) A. D. Becke, *J. Chem. Phys.* **1992**, *97*, 9173-9177; d) A. D. Becke, *J. Chem. Phys.* **1993**, *98*, 5648-5652.

[37] V. N. Staroverov, G. E. Scuseria, J. Tao, and J. P. Perdew, *J. Chem. Phys.*, **2003**, *119*, 12129–12137.

[38] A. Schaefer, H. Horn, R. J. Ahlrichs, *J. Chem. Phys.* **1992**, *97*, 2571-2577.

[39] A. Schaefer, H. Horn, R. J. Ahlrichs, *J. Chem. Phys.* **1994**, *100*, 5829-5835.

[40] M. Romelt, S. Ye, F. Neese, *Inorg. Chem.* **2009**, *48*, 784-757.

[41] Gaussian 16, Revision A.03, M. J. Frisch, G. W. Trucks, H. B. Schlegel, G. E. Scuseria, M. A. Robb, J. R. Cheeseman, G. Scalmani, V. Barone, G. A. Petersson, H. Nakatsuji, X. Li, M. Caricato, A. V. Marenich, J. Bloino, B. G. Janesko, R. Gomperts, B. Mennucci, H. P. Hratchian, J. V. Ortiz, A. F. Izmaylov, J. L. Sonnenberg, D. Williams-Young, F. Ding, F. Lipparini, F. Egidi, J. Goings, B. Peng, A. Petrone, T. Henderson, D. Ranasinghe, V. G. Zakrzewski, J. Gao, N. Rega, G. Zheng, W. Liang, M. Hada, M. Ehara, K. Toyota, R. Fukuda, J. Hasegawa, M. Ishida, T. Nakajima, Y. Honda, O. Kitao, H. Nakai, T. Vreven, K. Throssell, J. A. Montgomery, Jr., J. E. Peralta, F. Ogliaro, M. J. Bearpark, J. J. Heyd, E. N. Brothers, K. N. Kudin, V. N. Staroverov, T. A. Keith, R. Kobayashi, J. Normand, K. Raghavachari, A. P. Rendell, J. C. Burant, S. S. Iyengar, J. Tomasi, M. Cossi, J. M. Millam, M. Klene, C. Adamo, R. Cammi, J. W. Ochterski, R. L. Martin, K. Morokuma, O. Farkas, J. B. Foresman, D. J. Fox, Gaussian, Inc., Wallingford CT, **2016**.

[42] a) T. H. Dunning, Jr., P. J. Hay, in Modern Theoretical Chemistry; Plenum: New York,**1977**, Vol. 3, pp 1– 28; b) P. Fuentealba, H. Preuss, H. Stoll, L. Vonszentpaly, Chem. Phys. Lett. **1982**, *89*, 418-422.

[43] a) A. Schaefer, H. Horn, R. Ahlrichs, *J. Chem. Phys.*, **1992**, *97*, 2571-2577; b) A. Schaefer, C. Huber, R. Ahlrichs, *J. Chem. Phys.*, **1994**, *100*, 5829-5835.

Entry for the Table of Contents (Please choose one layout)

FULL PAPER

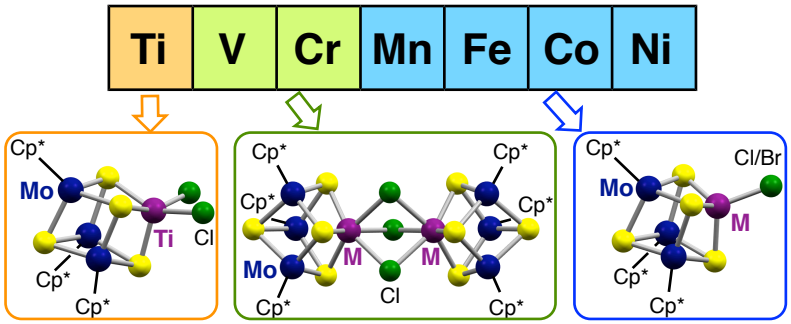

Yasuhiro Ohki, Keisuke Uchida, Ryota Hara, Mami Kachi, Mayu Fujisawa, Mizuki Tada, Yoichi Sakai, W. M. C. Sameera*、

Page No. – Page No.

Cubane-Type $[Mo_3S_4M]$ Clusters with First-Row Group 4-10 Transition-Metal Halides Supported by C_5Me_5 Ligands on Molybdenum

Text for Table of Contents

A synthetic protocol was developed for a series of cubane-type $[Mo_3S_4M]$ clusters, based on the anionic cluster platform $[Cp^*{}_3Mo_3S_4]^-$, that incorporate halides of first-row transition metals from group 4-10 (M). The M:halide ratio gradually increases from 1:2 to 1:1.5 and to 1:1 upon moving from early to late transition metals.